ACS APPLIED MATERIALS & INTERFACES

Research Article

www.acsami.org

Aggregation-Induced-Emissive Molecule Incorporated into Polymeric Nanoparticulate as FRET Donor for Observing Doxorubicin Delivery

Xiongqi Han,[†] De-E Liu,[†] Tieyan Wang,[†] Hongguang Lu,[†] Jianbiao Ma,[†] Qixian Chen,[*,‡] and Hui Gao[*,†]

[†]School of Chemistry and Chemical Engineering, Tianjin Key Laboratory of Organic Solar Cells and Photochemical Conversion, Tianjin University of Technology, Tianjin 300384, China

[‡]Department of Chemistry, Massachusetts Institute of Technology, Cambridge, Massachusetts 02139, United States

Supporting Information

ABSTRACT: Tetraphenylethene (TPE) derivatives characterized with distinct aggregation-induced-emission, attempted to aggregate with doxorubicin (Dox) to formulate the interior compartment of polymeric nanoparticulate, served as fluorescence resonance energy transfer (FRET) donor to promote emission of acceptor Dox. Accordingly, this FRET formulation allowed identification of Dox in complexed form by detecting FRET. Important insight into the Dox releasing can be subsequently explored by extracting complexed Dox (FRET) from the overall Dox via direct single-photon excitation of Dox. Of note, functional catiomers were used to complex with FRET partners for a template formulation, which was verified to induce pH-responsive release in the targeted subcellular compartment. Hence, this well-defined multifunctional system entitles in situ observation of the drug releasing profile and insight on drug delivery journey from the tip of injection vein to the subcellular organelle of the targeted cells.

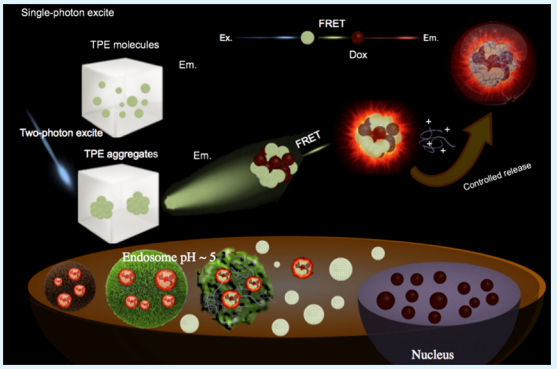

KEYWORDS: *aggregation-induced-emission, tetraphenylethene (TPE), poly(glycerol methacrylate) (PGMA), FRET, two-photon excitation, tumor target*

Doxorubicin (Dox) as extensively prescribed as anticancer chemotherapy drug, routinely administered into the vein, has been verified to impose severe irritations because of its propensity to leak into the surrounding tissue of the administration site and nonspecific accumulation into vital organs.[1,2] To circumvent the poor bioavailability issue, appropriate manufacture of nanoscale delivery vehicle to encapsulate the Dox cargo is plausible to acquire improved bioavailability to the tumors and reduced nonspecific toxicities.[3−7] Nevertheless, detailed information regarding to in situ Dox transportation scenario post systemic administration and subsequent intracellular trafficking is elusive owing to the restriction presented by intrinsic nature of Dox, its hydrophobicity leads to substantial aggregation induced quenching to the coupled fluorescence reporter.[8] However, lacking of these critical information will impose substantial obstacle to acquire prognosis and impede the verification of the developing strategies in pursuit of improved therapeutic efficacy. An ultimate modality for drug delivery should, ensemble of both therapeutic and reporting functionalities, be capable of not only affording targeted delivery activity, efficient cellular uptake, controlled intracellular drug releasing, but also providing facile functionality for in situ supervision of the encapsulated drug cargo over the whole process of drug delivery.[9−12] To accomplish this task, tetraphenylethene (TPE), a novel fluorophore characterized with distinctive aggregation induced emission (AIE) behavior,[13−16] was utilized to construct interior of drug delivery vehicle via hydrophobic aggregation with Dox.[17,18] In this report, *para*-carboxyl-functionalized TPE was synthesized, exhibiting excellent solubility in aqueous phosphate buffered saline (PBS, pH 7.4). This is particularly desirable to the biological applications, which could resolve the potential safety issues related to organic solvents, e.g. DMSO, required to dissolve TPE.[18] Importantly, the emission wavelength of TPE coincided with the wavelength requested by excitation of Dox.[18] Accordingly, TPE can be anticipated to not only serve as amplifier to promote in situ surveillance of doxorubicin based on fluorescence resonance energy transfer (FRET) between TPE (donor) and Dox (acceptor) with respect to the critical distance requirement for FRET (within 10 nm),[19] but also as reporter to disclose the drug-releasing site, the destination of the carrier and the executing site of the drugs at subcellular level.[20−22] To test our strategy, we attempted to create a template formulation here for possible

Received: September 1, 2015
Accepted: October 8, 2015
Published: October 8, 2015

DOI: 10.1021/acsami.5b08202
ACS Appl. Mater. Interfaces 2015, 7, 23760−23766

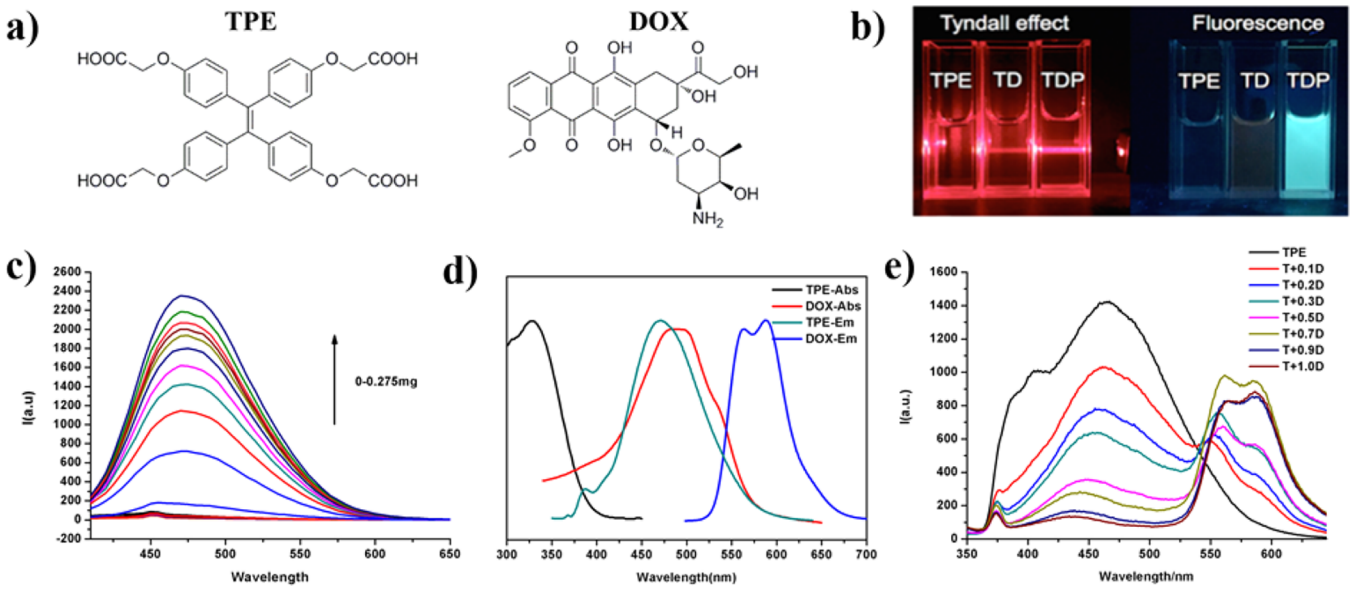

Figure 1. Validation of TPE and Dox as combinatorial duo for potential utility in surveillance of Dox based on characteristic AIE behavior of donor TPE and FRET to acceptor Dox. (a) Chemical structure of TPE and Dox. (b) Tyndall effect and fluorescence emission of TPE, TD, and TDP. (c) Distinctive AIE behavior of TPE, where TPE solution at constant concentration complexed with varying concentration of PGMA-EDA was excited at wavelength of 330 nm. (d) Characterization of absorbance and emission profile of TPE and Dox. (e) Distinctive FRET spectra of TPE/Dox mixture, where TPE solution at constant concentration mixed with varying concentration of Dox was excited at wavelength of 330 nm.

utility in surveillance of Dox delivery. Specifically, TPE/Dox interior was created based on aggregation of their hydrophobic components, and the anionic carboxyl functionalization to TPE enable subsequent electrostatic complexation with pH responsive cationic amino poly(glycerol methacrylate) (PGMA) derivative to seek controlled intracellular Dox releasing.[23−25] The abundant amino groups of PGMA derivative is convenient for further chemistry functionalization, herein ligand folic acid was introduced with aim of improved tumor targeting function.[26] Of note, previous research has demonstrated the strategic introduction of folic acid into charged components capable of overcoming the difficulty of the exposure of lipophilic folic acid, thereby facilitating receptor-mediated interaction.[27] Pertaining to the optimal wavelength (~330 nm) to excite TPE in UV region, we were encouraged to employ an alternative red-shifted two-photon excitation for acquiring deeper tissue penetration, efficient light detection, and reduced phototoxicity. The facile combinatorial strategy of AIE and FRET would permit identification of aggregated form of Dox (aggregated with TPE in the complex) by observing FRET emission via two-photon excitation of TPE. Furthermore, the overall Dox was captured via direct single-photon excitation of Dox, consequently providing important implication of the released Dox. In this regard, it can be anticipated that the constructed Dox delivery vehicle should provide an intriguing platform for targeted delivery of Dox with appreciable surveillance capacity, allowing in situ observing delivery scenario from the range of the whole living body to the subcellular level.

To start with, the functional components (chemical structures in Figure 1a) in the proposed formulation were synthesized. The TPE derivative characterized with anionic carboxyl groups was synthesized according to scheme 1 (Figure S1). The resulting product was characterized by ^{1}H NMR, ^{13}C NMR, and DEPT$_{135}$ measurement, and the peaks of the ^{1}H NMR, ^{13}C NMR, and DEPT$_{135}$ spectra were correctly assigned to the corresponding protons and carbons of TPE-COOH, indicating successful carboxyl functionalization to TPE (TPE-COOH was referred as TPE hereafter). Furthermore, the cationic PGMA derivative was synthesized according to scheme 2 (Figure S2).[28,29] The resulting product of PGMA (M_n = 13 000, polydispersity = 1.20, as determined by GPC) was characterized by ^{1}H NMR measurement, and the peaks of the ^{1}H NMR spectral were well-assigned to the corresponding protons of PGMA. The epoxy groups of PGMA were then reacted with ethylenediamine to obtain cationic amino PGMA (PGMA-EDA)[30−32] and its amination conversion ratio was determined to be 81.6% according to elemental analysis. Furthermore, the folic acid conjugation to the side chain of PGMA-EDA was performed by coupling reaction of carboxyl groups from folic acid and amine groups from PGMA precursor, the successful conjugation of folic acid was confirmed by IR and fluorescence measurement (Figure S2), which was determined to possess 5.5 folic acid per PGMA precursor.

Prior to nanoparticle fabrication, it is important to confirm the yielded TPE capable of preserving AIE character. No distinct Tyndall effect was observed for TPE in PBS solution (pH 7.4) (Figure 1b), indicating its excellent molecular dispersion in aqueous solution. In consistency, the fluorescence emission of this pure TPE solution was measured to be markedly low as compared to the mixture of TPE and cationic PGMA-EDA (Figure 1c). The fluorescence emission of TPE appeared to follow progressive enhancement with continuous addition of PGMA-EDA (Figure 1c), likely to be a consequence of TPE aggregation with cationic PGMA-EDA through electrostatic complexation. This result verified TPE preserving appreciable AIE character despite it having been para-functionalized with carboxyl groups. The validation of TPE with distinct AIE character implied its potential use to promote excitation of its interior partner Dox based on FRET.

Furthermore, recording of the excitation and emission spectra for TPE and Dox verified them as the appreciable

DOI: 10.1021/acsami.5b08202
ACS Appl. Mater. Interfaces 2015, 7, 23760−23766

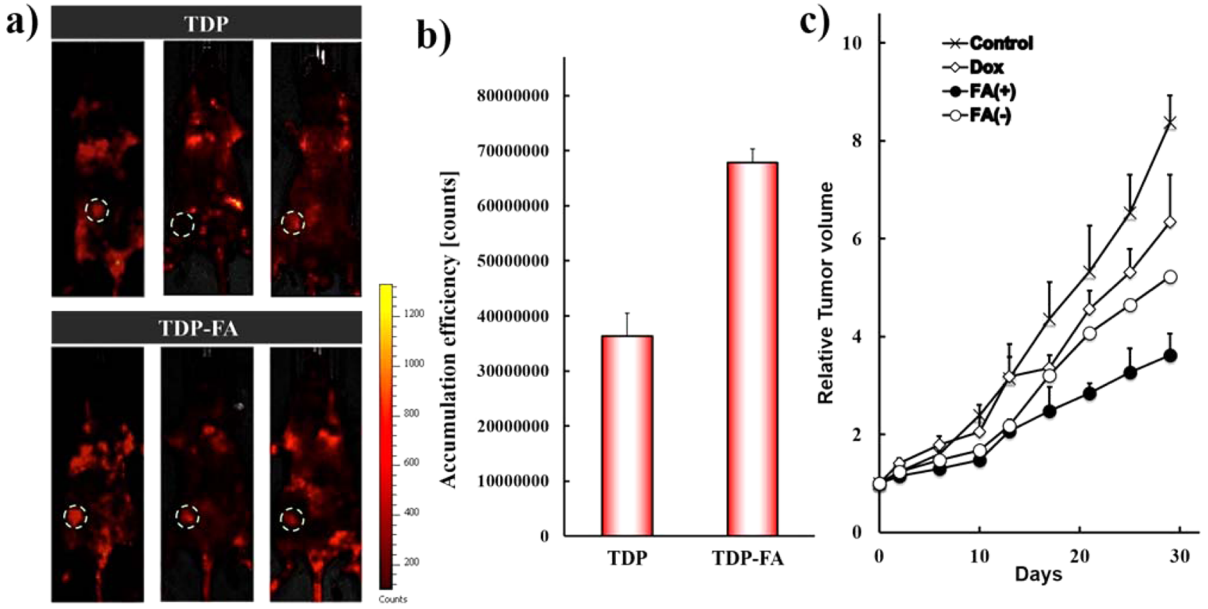

Figure 2. In vivo systemic performances of TDP and TDP-FA to HeLa tumor bearing mice. (a) Biodistribution profiles of Dox was investigated by IVIS for the samples of TDP and TDP-FA, where the quantified data for tumor accumulation was summarized as bar graph (b). (c) Tumor suppression potency of TDP and TDP-FA via intravenous administration to HeLa tumor bearing mice, where molecular Dox and blank PBS served as control samples, $n = 6$. (**$p < 0.01$; Student's t test).

combinatorial duo to establish the FRET system, where the emission range of donor TPE (400−570 nm) almost coincided with the excitation range of acceptor Dox (350−600 nm), (Figure 1d). Subsequent recording the excitation/emission spectra of TPE and Dox mixture (constant TPE concentration but varying Dox concentration) captured distinct character of FRET: progressive growth in emission at wavelength of 580 nm (emission of acceptor Dox) in accompany with the gradually decline in emission at wavelength of 450 (emission of donor TPE) (Figure 1e). In addition, the excitation spectra DOX was measured at the emission wavelength of DOX (580 nm). The maximum excitation wavelength of DOX was determined as 490 nm (Figure S3), which is consistent with emission wavelength of TPE, suggesting the occurrence of FRET. On the other hand, the fluorescence lifetime of TPE is 439.7 ns. In contrast, when formed NPs, the lifetime of TPE was significantly decreased to 287.2 ns (Table S1), which further confirmed the existence of FRET process in the NPs, because the occurrence of FRET usually accompanied by a shortened fluorescence lifetime of the donor.[33]

To fabricate nanoparticle with interior composed of TPE and Dox (referred hereafter as TD), TPE and Dox stock solutions were prepared by dissolved the powder in PBS (pH 7.4), respectively. Then, an aliquot of 50 μL of TPE in PBS was applied to 40 μL of Dox aqueous solution under vortex. Aiming for a controlled release of Dox, the pH responsive PGMA-EDA was electrostatically complexed with preformed TD interior to formulate the exterior layer, which was referred hereafter as TDP. The attachment of PGMA-EDA was confirmed by zeta-potential measurement, where negative zeta-potential of TD (−17.4 mV) was determined to transformed +20.1 mV upon addition of PGMA-EDA (Figure S4a). In consistency, distinct Tyndall effect was observed for TD and TDP, particular for TDP (Figure 1b), indicating the defined aggregated structure of TDP. To demonstrate the feasibility of the proposed system capable of promoting emission of aggregated Dox, laser light at a wavelength of 365 nm was used to excite the solution of TPE, TD and TDP. As opposed to limited emission of TPE solution, intense emission was observed for the TDP complexes, which can be explained by the aggregation of Dox and TPE. The obtained results validated the potential use of AIE of TPE to promote the traceability of Dox.

Aiming for tumor-targeted delivery, folic acid, whose receptors were abundantly overexpressed on the tumor cells, was introduced into the side chain of PGMA-EDA (PGMA-FA) as alternative PGMA-EDA to construct the exterior layer, which was referred hereafter as TDP-FA. The formed structures were characterized by scanning electron microscope (SEM) measurement. Uniform spherical structures were observed with approximate diameter of 40 nm (Figure S4b), which was poised to be within the optimal size range for systemic tumor therapy.[34] To demonstrate the potential use of the proposed system for tumor targeted delivery, the biodistribution of TDP and TDP-FA was investigated by in vivo imaging system (IVIS), as shown in Figure 2a and b, distinct prompted tumor accumulation (HeLa tumor) was observed for TDP-FA sample, which verified the functional role of FA in prompting tumor targeted delivery. In consistency, the systemic treatment of subcutaneous xenografted HeLa tumor approved the improved potency of TDP-FA sample than TDP sample (Figure 2c), thereby verifying the strategic use of folic acids for improved delivery of drug cargo to the tumors. In vitro cellular uptake evaluation provided evidence of the improved accumulation as a result of the increased specific affinity of folic acid to its receptors. Pronounced enhancement in cellular uptake was observed for TDP-FA sample as compared to TDP sample in HeLa cells (overexpression of folic acid receptors) (Figure 3a). Of note, the difference in cellular uptake of PGMA and PGMA-FA in A549 cells (limited expression of folic acid receptors) was not marked (Figure 3b), which affirmed the strategic use of folic acid to introduce specific affinity to the tumor cells to pursue promoted delivery of Dox into the tumor cells. Subsequence to cellular uptake, the nanoparticles was subjected to acidic digestive endosome/lysosome entrapment, thereby

DOI: 10.1021/acsami.5b08202
ACS Appl. Mater. Interfaces 2015, 7, 23760−23766

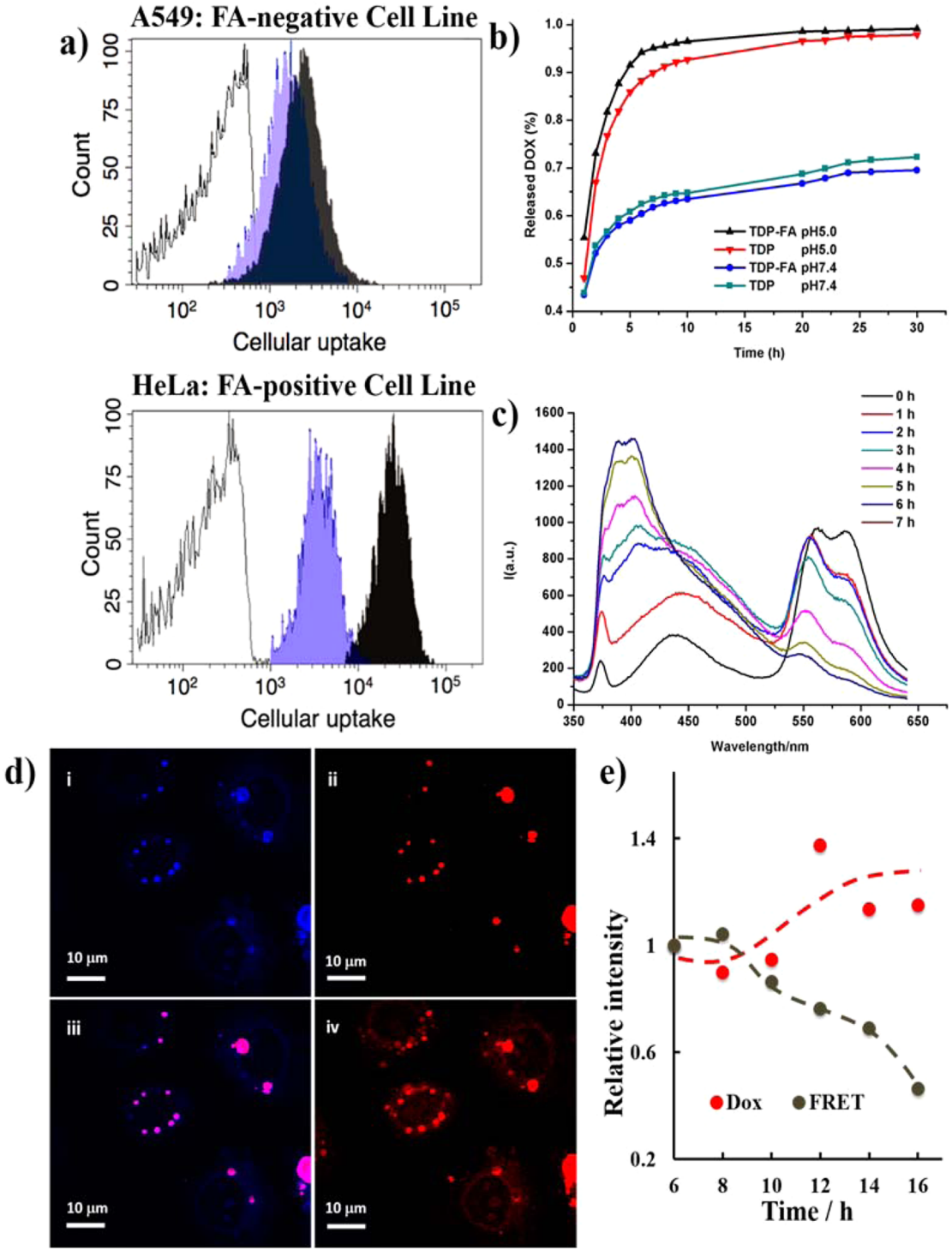

Figure 3. Cellular Uptake and intracellular trafficking activity of molecular Dox, TDP, and TDP-FA. (a) Flow Cytometry evaluation of cellular uptake efficiency of TDP and TDP-FA in FA-receptor-positive cell line of HeLa cells and FA-receptor-negative control cell line of A549 cells (white: blank cells, purple: TDP, black: TDP-FA). (b) Real-time Dox releasing profile at pH 7.4 and pH 5.0 buffer. (c) Derivation of emission spectra in response to Dox releasing, where the emission profile of TDP sample was measured at a time dependent manner under excitation with wavelength of 330 nm. (d) CLSM observation to distinguish intracellular distribution of Dox. (i) TPE (two-photon excitation of TPE); (ii) aggregated Dox complex (FRET through two-photon excitation of TPE); (iii) image of panels i and ii merged; (iv) overall Dox (single-photon excitation of Dox). Scale bar: 10 μm. (e) Insight on drug releasing profile in HeLa cells through in vitro quantification of FRET of TDP-FA as a function of incubation time starting from 6 h post transfection under excitation of 330 nm and emissions of 580−620 nm.

requested the necessity of retrieve the entrapment of nanoparticles from endosome entrapment.

To serve these purposes, the strategic use of the pH responsive PGMA-EDA was investigated. As demonstrated previously, PGMA-EDA has exhibited appreciable endosome escape function due to its facilitated protonation at acidic endosome pH 5.5 than physiological pH 7.4. Here, efforts were focused to clarify the promoted intracellular releasing of the

DOI: 10.1021/acsami.5b08202
ACS Appl. Mater. Interfaces 2015, 7, 23760−23766

Dox with aids of PGMA-EDA. The experimental investigations verified the facilitated releasing of Dox at acidic endosome pH 5.5 as compared to pH 7.4 (Figure 3b,c). Most likely, the charge unbalance of electrostatic assembled structure was induced due to promoted protonation of PGMA-EDA, thus resulting in structural rearrangement to release excess cationic components of PGMA-EDA in the acidic endosome, which is likely then associate with negative-charged endosome membrane to induce membrane disruption and further endosome escape. Furthermore, the released nanostructures to the cytosol (pH 7.4) became excess negative charge, thus undergoing further structural rearranging to facilitate release of anionic TPE together with its interior partner Dox. The obtained results suggest the potential use of pH responsive PGMA-EDA for endosome escape and intracellular drug release.

To explore direct insight on the Dox releasing behavior, we conducted confocal laser scanning microscopy (CLSM) observation by means of two-photon excitation of TPE to visualize aggregated-Dox through FRET and single-photon excitation of Dox to screen the overall intracellular Dox. As shown in Figure 3d, the aggregated Dox complex observed to reside in spherical subcellular compartment (endosome) with intense brightness, verified efficiency of combinatorial use of AIE and FRET for detection of aggregated Dox. In addition, minor fraction of the aggregated Dox complex was observed in the cytosol, suggesting the readily dissociation of complex and Dox releasing occurred largely in the acidic endosome by virtue of pH-responsive PGMA-EDA. No observable aggregated Dox complex was in the nucleus, consistent with the fact that the nucleus membrane representing as barrier to restrict the entry of irrelevant macromolecules or nanoparticulates. Virtually, all substances are requested to translocate the nuclear membrane through nuclear pore complex (NPC), and transport across the NPC has been reviewed in detail.[35−42] Small molecules, such as ions, metabolites, and intermediate-sized macromolecules, can pass unassisted by diffusion which becomes increasingly restricted as the particle approaches a size limit of ∼10 nm in diameter.[43,44] Consequently, it is not possible to observe the localization of the aggregated Dox complex (approximate 40 nm in diameter) in the nucleus. On the other hand, the overall intracellular Dox was screened under single-photon excitation of Dox. Aside from the aforementioned endosome-entrapped aggregated Dox complex, there was marked extra Dox presenting in the cytosol and nucleus, presumed to ascribe to the molecular Dox released from the complex. These results validated the potential use of the AIE and FRET for insight on the intracellular delivery and releasing behavior of the Dox delivery system. Furthermore, to establish quantification of intracellular Dox releasing rate of the proposed system, the intensity of FRET post transfection was recorded. Presumably, consistent decrease of FRET should be accompanied by Dox releasing. The prior estimation has validated readily Dox releasing at pH 5.5 (mimicking endosome) as compared to pH 7.4 (Figure 3b), supporting the assumption of preferable releasing of Dox in the endosome. The FRET recording witnessed gradually lowered FRET intensity with extension of incubation time (Figure 3c), implying FRET can be employed as an indicator to quantify the releasing profile of the encapsulated Dox. In vitro time-dependent measuring the FRET intensity of TPE/Dox approved the readily releasing of Dox and TPE from the nanoparticles, where FRET intensity appeared to undergo consistent decrease with extended incubation (Figure 3d). Hence, these results affirmed the potential of TPE to trace or quantify the releasing rate of Dox-loaded delivery system. Another noteworthy was the capacity of the proposed system to demonstrate segregated intracellular distribution of donor TPE and acceptor Dox after releasing. These intriguing observations inspire tremendous utilities of the proposed system in understanding drug delivery kinetics and intracellular delivery scenario. Furthermore, aside from appreciable drug delivery efficiency, the synthetic components used in fabrication of the proposed system was verified to possess tempting safety profile, as evidenced in minimal cytotoxicity observed for nondrug TP sample composed of TPE and PGMA-EDA (Figure S5). Hence, the proposed system fabricated with biocompatible materials, providing critical functionalities with in situ surveillance of drug targeted and controlled delivery, thus should be emphasized in broad applications.

In summary, this study reports an appreciable drug delivery vehicle, ensemble of therapeutic and reporting functionalities. Aggregation of Dox and TPE created interior for subsequent attachment of external PGMA-EDA, which elicited functions of endosome escape and controlled intracellular Dox releasing. Targeted tumor delivery was achieved by introducing ligand folic acids at the side chain of PGMA-EDA, thus resulting in potent therapeutic efficacy. Noteworthy is strategic use of TPE whose distinct AIE entitled the potential use in surveillance of systemic Dox delivery. Intracellular releasing profile could also be dissected with regard to the distance limitation for FRET. Pertaining to the relative short wavelength (UV range) to excite TPE, two-photon excitation technique is particular applicable for the proposed system with respect to the potentials of high contrast, deep tissue penetration and reduced phototoxicity. Thus, the proposed system may provide an important platform to pursue in situ tracing drug delivery and gain the detailed scenario from the tip of injection vein to the subcellular organelle of the targeted cells.

■ ASSOCIATED CONTENT

Supporting Information

The Supporting Information is available free of charge on the ACS Publications website at DOI: 10.1021/acsami.5b08202.

Synthetic procedure and product characterization, zeta potential measurement, SEM observation, cytotoxicity, together with all the detailed experiment procedures (PDF)

■ AUTHOR INFORMATION

Corresponding Authors

*E-mail: qixian@mit.edu.

*E-mail: hgao@tjut.edu.cn.

Author Contributions

The manuscript was written through contributions of all authors. All authors have given approval to the final version of the manuscript.

Notes

The authors declare no competing financial interest.

■ ACKNOWLEDGMENTS

The authors would like to thank National Natural Science Foundation of China (21374079, 21244004), Program for New Century Excellent Talents in University (NCET-11-1063), and Program for Prominent Young College Teachers of Tianjin Educational Committee for financial support.

DOI: 10.1021/acsami.5b08202
ACS Appl. Mater. Interfaces 2015, 7, 23760−23766

REFERENCES

(1) Hayek, E. R.; Speakman, E.; Rehmus, E. Acute doxorubicin cardiotoxicity. *N. Engl. J. Med.* **2005**, *352*, 2456−2457.

(2) Fundarò, A.; Cavalli, R.; Bargoni, A.; Vighetto, D.; Zara, G. P.; Gasco, M. R. Non-stealth and stealth solid lipid nanoparticles (SLN) carrying doxorubicin: pharmacokinetics and tissue distribution after i.v. administration to rats. *Pharmacol. Res.* **2000**, *42*, 337−343.

(3) Gabizon, A.; Shmeeda, H.; Barenholz, Y. Pharmacokinetics of pegylated liposomal Doxorubicin: review of animal and human studies. *Clin. Pharmacokinet.* **2003**, *42*, 419−436.

(4) Kataoka, K.; Matsumoto, T.; Yokoyama, M.; Okano, T.; Sakurai, Y.; Fukushima, S.; Okamoto, K.; Kwon, G. S. Doxorubicin-loaded poly(ethylene glycol)-poly(beta-benzyl-L-aspartate) copolymer micelles: their pharmaceutical characteristics and biological significance. *J. Controlled Release* **2000**, *64*, 143−153.

(5) Chiang, Y.-T; Lo, C.-L. pH-responsive polymer-liposomes for intracellular drug delivery and tumor extracellular matrix switched-on targeted cancer therapy. *Biomaterials* **2014**, *35*, 5414−5424.

(6) Yoo, H. S.; Park, T. G. Biodegradable polymeric micelles composed of doxorubicin conjugated PLGA-PEG block copolymer. *J. Controlled Release* **2001**, *70*, 63−70.

(7) Yan, Y.; Johnston, A. P.; Dodds, S. J.; Kamphuis, M. M.; Ferguson, C.; Parton, R. G.; Nice, E. C.; Heath, J. K.; Caruso, F. Uptake and Intracellular Fate of Disulfide-Bonded Polymer Hydrogel Capsules for Doxorubicin Delivery to Colorectal Cancer Cells. *ACS Nano* **2010**, *4*, 2928−2936.

(8) Watson, P.; Jones, A. T.; Stephens, D. J. Intracellular trafficking pathways and drug delivery: fluorescence imaging of living and fixed cells. *Adv. Drug Delivery Rev.* **2005**, *57*, 43−61.

(9) Liu, Y.; Miyoshi, H.; Nakamura, M. Nanomedicine for drug delivery and imaging: a promising avenue for cancer therapy and diagnosis using targeted functional nanoparticles. *Int. J. Cancer* **2007**, *120*, 2527−2537.

(10) Ling, D.; Park, W.; Park, S.-J.; Lu, Y.; Kim, K. S.; Hackett, M. J.; Kim, B. H.; Yim, H.; Jeon, Y. S.; Na, K. Multifunctional tumor pH-sensitive self-assembled nanoparticles for bimodal imaging and treatment of resistant heterogeneous tumors. *J. Am. Chem. Soc.* **2014**, *136*, 5647−5655.

(11) Huang, C. K.; Lo, C. L.; Chen, H. H.; Hsiue, G. H. Multifunctional micelles for cancer cell targeting, distribution imaging, and anticancer drug delivery. *Adv. Funct. Mater.* **2007**, *17*, 2291−2297.

(12) Yang, Z.; Lee, J. H.; Jeon, H. M.; Han, J. H.; Park, N.; He, Y.; Lee, H.; Hong, K. S.; Kang, C.; Kim, J. S. Folate-based near-infrared fluorescent theranostic gemcitabine delivery. *J. Am. Chem. Soc.* **2013**, *135*, 11657−11662.

(13) Wang, M.; Zhang, G.; Zhang, D.; Zhu, D.; Tang, B. Z. Fluorescent bio/chemosensors based on silole and tetraphenylethene-luminogens with aggregation-induced emission feature. *J. Mater. Chem.* **2010**, *20*, 1858−1867.

(14) Tong, H.; Hong, Y.; Dong, Y.; Häussler, M.; Li, Z.; Lam, J. W.; Dong, Y.; Sung, H. H.; Williams, I. D.; Tang, B. Z. Protein detection and quantitation by tetraphenylethene-based fluorescent probes with aggregation-induced emission characteristics. *J. Phys. Chem. B* **2007**, *111*, 11817−11823.

(15) Jiang, B.-P.; Guo, D.-S.; Liu, Y.-C.; Wang, K.-P.; Liu, Y. Photomodulated fluorescence of supramolecular assemblies of sulfonatocalixarenes and tetraphenylethene. *ACS Nano* **2014**, *8*, 1609−1618.

(16) Yuan, Y.; Kwok, R. T.; Tang, B. Z.; Liu, B. Targeted theranostic platinum(IV) prodrug with a built-in aggregation-induced emission light-up apoptosis sensor for noninvasive early evaluation of its therapeutic responses in situ. *J. Am. Chem. Soc.* **2014**, *136*, 2546−2654.

(17) Zhang, C.; Jin, S.; Li, S.; Xue, X.; Liu, J.; Huang, Y.; Jiang, Y.; Chen, W.-Q.; Zou, G.; Liang, X.-J. Imaging Intracellular Anticancer Drug Delivery by Self-Assembly Micelles with Aggregation-Induced Emission (AIE Micelles). *ACS Appl. Mater. Interfaces* **2014**, *6*, 5212−5220.

(18) Xue, X.; Zhao, Y.; Dai, L.; Zhang, X.; Hao, X.; Zhang, C.; Huo, S.; Liu, J.; Liu, C.; Kumar, A.; Chen, W.; Zou, G.; Liang, X. Spatiotemporal drug release visualized through a drug delivery system with tunable aggregation-induced emission. *Adv. Mater.* **2014**, *6*, 712−717.

(19) Patterson, G. H.; Piston, D. W.; Barisas, B. G. Förster distances between green fluorescent protein pairs. *Anal. Biochem.* **2000**, *284*, 438−440.

(20) Xue, X.; Jin, S.; Zhang, C.; Yang, K.; Huo, S.; Chen, F.; Zou, G.; Liang, X.-J. Probe-Inspired Nano-Prodrug with Dual-Color Fluorogenic Property Reveals Spatiotemporal Drug Release in Living Cells. *ACS Nano* **2015**, *9*, 2729−2739.

(21) Yu, J.-C.; Chen, Y.-L.; Zhang, Y.-Q.; Yao, X.-K.; Qian, C.-G.; Huang, J.; Zhu, S.; Jiang, X.-Q.; Shen, Q.-D.; Gu, Z. pH-Responsive and Near-Infrared-Emissive Polymer Nanoparticles for Simultaneous Delivery, Release, and Fluorescence Tracking of Doxorubicin in Vivo. *Chem. Commun.* **2014**, *50*, 4699−4702.

(22) Li, S.-Y.; Liu, L.-H.; Cheng, H.; Li, B.; Qiu, W.-X.; Zhang, X.-Z. A Dual-FRET-based Fluorescence Probe for the Sequential Detection of MMP-2 and Caspase-3. *Chem. Commun.* **2015**, *51*, 14520−14523.

(23) Gu, W.; Li, Q.; Lu, H.; Fang, L.; Chen, Q.; Yang, Y.; Gao, H. Construction of stable polymeric vesicles based on azobenzene and beta-cyclodextrin grafted poly(glycerol methacrylate)s for potential applications in colon-specific drug delivery. *Chem. Commun.* **2015**, *51*, 4715−4718.

(24) Li, Q.; Wang, L.; Qiu, X.; Sun, Y.; Wang, P.; Liu, Y.; Li, F.; Qi, A.; Gao, H.; Yang, Y. Stimuli-responsive biocompatible nanovalves based on β-cyclodextrin modified poly (glycidyl methacrylate). *Polym. Chem.* **2014**, *5*, 3389−3395.

(25) Li, Q.; Gu, W.; Gao, H.; Yang, Y. Self-assembly and applications of poly(glycidyl methacrylate)s and their derivatives. *Chem. Commun.* **2014**, *50*, 13201−13215.

(26) Low, P. S.; Henne, W. A.; Doorneweerd, D. D. Discovery and development of folic-acid-based receptor targeting for imaging and therapy of cancer and inflammatory diseases. *Acc. Chem. Res.* **2008**, *41*, 120−129.

(27) Li, L.; Yang, Q.; Zhou, Z.; Zhong, J.; Huang, Y. Doxorubicin-loaded, charge reversible, folate modified HPMA copolymer conjugates for active cancer cell targeting. *Biomaterials* **2014**, *35*, 5171−5187.

(28) Gao, H.; Jones, M.; Chen, J.; Liang, Y. R.; Prudhomme, R. E.; Leroux, J. Hydrophilic nanoreservoirs embedded into polymeric nanoparticles - An approach to compatibilize polar molecules with hydrophobic matrices. *Chem. Mater.* **2008**, *20*, 4191−4193.

(29) Gao, H.; Jones, M.; Chen, J.; Prudhomme, R. E.; Leroux, J. Core cross-linked reverse polymeric micelles. *Chem. Mater.* **2008**, *20*, 3063−3067.

(30) Li, C.; Yang, Y.; Liang, Z.; Wu, G.; Gao, H. Post-modification poly(glycidyl methacrylate)s with alkyl amine and isothiocyanate for effective pDNA delivery. *Polym. Chem.* **2013**, *4*, 4366−4374.

(31) Liang, Z.; Wu, X.; Yang, Y.; Li, C.; Wu, G.; Gao, H. Quaternized amino poly(glycerol-methacrylate)s for enhanced pDNA deliver. *Polym. Chem.* **2013**, *4*, 3514−3523.

(32) Gao, H.; Elsabahy, M.; Giger, E. V.; Li, D. K.; Prudhomme, R. E.; Leroux, J. C. Aminated linear and star-shape poly(glycerol methacrylate)s: synthesis and self-assembling properties. *Biomacromolecules* **2010**, *11*, 889−895.

(33) Cheng, S.-H.; Chen, N.-T.; Wu, C.-Y.; Chung, C.-Y.; Hwu, Y.; Mou, C.-Y.; Yang, C.-S.; Lo, L.-W. Recent Advances in Dynamic Monitoring of Drug Release of Nanoparticle Using Forster Resonance Energy Transfer and Fluorescence Lifetime Imaging. *J. Chin. Chem. Soc.* **2011**, *58*, 798−804.

(34) Cabral, H.; Matsumoto, Y.; Mizuno, K.; Chen, Q.; Murakami, M.; Kimura, M.; Terada, Y.; Kano, M. R.; Miyazono, K.; Uesaka, M.; Nishiyama, N.; Kataoka, K. Accumulation of sub-100 nm polymeric micelles in poorly permeable tumours depends on size. *Nat. Nanotechnol.* **2011**, *6*, 815−823.

(35) Corbett, A. H.; Silver, P. A. Nucleocytoplasmic Transport of Macromolecules. *Microbiol. Mol. Biol. R.* **1997**, *61*, 193−211.

(36) Mattaj, I. W.; Englmeier, L. Nucleocytoplasmic Transport: The Soluble Phase. *Annu. Rev. Biochem.* **1998**, *67*, 265−306.

DOI: 10.1021/acsami.5b08202
ACS Appl. Mater. Interfaces 2015, 7, 23760−23766

(37) Gorlich, D.; Kutay, U. Transport Between the Cell Nucleus and the Cytoplasm. *Annu. Rev. Cell Dev. Biol.* **1999**, *15*, 607−660.
(38) Yoneda, Y. Nucleocytoplasmic protein traffic and its significance to cell function. *Genes Cells* **2000**, *5*, 777−787.
(39) Fried, H.; Kutay, U. Nucleocytoplasmic Transport: Taking an Inventory. *Cell. Mol. Life Sci.* **2003**, *60*, 1659−1688.
(40) Weis, K. Regulating Access to the Genome: Nucleocytoplasmic Transport throughout the Cell Cycle. *Cell* **2003**, *112*, 441−451.
(41) Suntharalingam, M.; Wente, S. R. Peering through the Pore: Nuclear Pore Complex Structure, Assembly, and Function. *Dev. Cell* **2003**, *4*, 775−789.
(42) Pemberton, L. F.; Paschal, B. M. Mechanisms of Receptor-Mediated Nuclear Import and Nuclear Export. *Traffic* **2005**, *6*, 187−198.
(43) Paine, P. L.; Moore, L. C.; Horowitz, S. B. Nuclear Envelope Permeability. *Nature* **1975**, *254*, 109−114.
(44) Keminer, O.; Peters, R. Permeability of Single Nuclear Pores. *Biophys. J.* **1999**, *77*, 217−228.

DOI: 10.1021/acsami.5b08202
ACS Appl. Mater. Interfaces 2015, 7, 23760−23766